Plasmonically Generated Tryptophan Radical Anion on Gold Nanoparticles Investigated by Combined Surface Enhanced Raman Scattering and Density Functional Theory Calculations.

Chelsea M. Zoltowski, Rémy F. Lalisse, Christopher M. Hadad, and Zachary D. Schultz* Department of Chemistry and Biochemistry, The Ohio State University, Columbus, OH 43210

*corresponding author email: schultz.133@osu.edu

Abstract:

Surface enhanced Raman scattering (SERS) offers increases in chemical sensitivity associated with the Raman signal from molecules interacting with plasmonic nanoparticles, and with use for diverse applications. This signal enhancement is the result of a combination of the enhanced electromagnetic field generated at the surface of the metal nanostructures and possible chemical enhancements specific to the molecule being detected. These chemical effects can alter the chemical identity of the analyte and manifest as differences in the SERS spectrum relative to the spontaneous Raman spectrum. In this work, we examine changes in the vibrational spectrum resulting from the previously hypothesized formation of a radical anion of the amino acid tryptophan on gold (Au) nanoparticles. Density functional theory (DFT) calculations are used to model changes in the vibrational frequencies attendant to the tryptophan radical anion and correlated with the experimentally observed vibrational modes in the SERS spectrum of tryptophan (Trp) on Au nanoparticles. The calculated vibrational frequencies are in close agreement with the experimental data. N-Acetyltryptophanamide (NATA) is shown to have the same trends in the calculated and experimental vibrations, indicating the captured electron is localized to the indole ring structure. Changes in the SERS spectrum with pH are readily explained by the calculations, further indicating the observed signal originates from the ground state radical anion in these experiments. This evidence for the capture of a hot electron by tryptophan and the resulting changes in the vibrational spectrum are important for molecular understanding of proteins and other molecules as detected by SERS.

Introduction:

Surface enhanced Raman scattering (SERS) is an evolving spectroscopic technique used to achieve the benefits of Raman while significantly enhancing the signal for trace detection. First observed on electrochemically roughened silver electrodes, the Raman enhancements have been shown to arise from localized plasmon resonances on nanoparticles and nanostructured materials. The confinement and re-radiation of the electric field on the surface of nanoparticles has become known as the electromagnetic enhancement mechanism, which explains the prevalence of SERS on plasmonic nanoparticles. In addition to the electromagnetic enhancement, chemical enhancements are also observed, where changes in the analyte molecule (e.g., charge-transfer resonances from adsorbed species) can provide additional signal enhancement from specific molecules.

The analyte-specific nature of the chemical enhancement is typically invoked to explain anomalous enhancements observed from specific analytes in the SERS field. The interaction between the analyte and the metal can alter the observed Raman frequencies in addition to contributing to the increased signal intensity. When analytes interact with a metal nanostructured surface, charge-transfer states can become accessible. These charge-transfer states may generate an additional resonance effect, dependent on the energy of the transition, resulting in surface enhanced resonance Raman scattering (SERRS) enhancements. Otto et al. noted the "first layer effect" which described the increased signal enhancement from molecules adsorbed directly to the metal surface. In addition to charge-transfer mechanisms, chemical enhancements have come to represent any analyte specific mechanisms that increase the SERS signal from the molecules.

Plasmon-excited, hot electrons can cause specific photochemical reactions on the surface of nanoparticles that may also alter the observed SERS signal. ¹⁰⁻¹¹ For example, the conversion of *para*-aminothiophenol (*p*-ATP) to 4,4'-dimercaptoazobenzene (DMAB) has been observed in SERS analysis, resulting from the excitation of energetic charge carriers in plasmonic particles. ¹²⁻¹³ The incident laser also generates high-energy electrons that promote chemical conversion. Zenobi et al. reported photo-fragmentation of analytes as a result of plasmonic hot-electrons. ¹⁴ Other reports have also shown anionic species resulting from plasmonic hot-electron transfer. ¹⁵⁻¹⁸ These chemical changes, while specific, have proven to be important in the interpretation and quantification of SERS spectra. The plasmon resonance involved with the more predictable electromagnetic enhancement can impact the chemical identity and the chemical enhancement

mechanisms. Photoproducts experience the increased electric field associated with the electromagnetic enhancement mechanism and give rise to the observed SERS signal.

The SERS analysis of proteins is reported to arise from several distinct interactions, such as plasmonic driven chemistry, fragmentation, and surface interactions. Studies have reported that aromatic amino acids are responsible for the most intense signals in SERS. ¹⁹⁻²⁰ These large aromatic side groups have been suggested to shield other parts of the protein in SERS. ²¹ The orientation of amino acids in short peptides and their interaction with the surface has also been investigated. ²² Differences in the SERS spectra from a specified protein on silver and gold nanostructures have previously been observed. ²³⁻²⁵ However, interpreting the SERS spectra of proteins and amino acids remains challenging.

Previous SERS studies of Trp interacting with a Au surface have largely been attributed spectral changes to surface adsorption interactions. It was reported that the indole ring has H-bonding interactions with negatively charged AuNPs;²⁶ however, a computational study showed the interation with the Au surface was favorable through either the carboxylic acid moiety or the pyrole ring.²⁷ A more recent work also noted SERS bands attributable to indole ring shifted, attributing these spectral changes to interactions between the gold surface and the indole ring.²⁸

Recently, we reported a series of experiments that suggest an alternative hypothesis for changes in the SERS spectrum of tryptophan on AuNPs.²⁹ We observed, using a combination of SERS, UV-Vis spectroscopy, and dynamic light scattering experiments, that the SERS signal from tryptophan correlated with exposure of the Trp-AuNPs suspension to the light at the plasmon resonance energy of the AuNPs (~532 nm) while SERS was obtained at a slightly off-resonant wavelength (633 nm). The UV-Vis and light scattering experiments, on the same samples, showed an electronic resonance in unaggregated particles that could be explained by electron capture by Trp molecules in close proximity to the AuNP surface, forming an anion radical. This hypothesis, that electron transfer to Trp is observed in the SERS spectrum, remains controversial.

There are many examples of using theory to explain the spectroscopically observed Raman signals. ^{22, 30-31} In SERS, this has been complicated by important aspects of the nanoparticles and the analyte molecule being intertwined. Indeed, efforts have attempted to provide a uniform theory of SERS; however, these explanations remain limited to subsets of molecules and interactions. ⁷ It is computationally challenging to simulate the full nanoparticle and analyte molecule in a

quantum mechanical treatment, and thus approximations are required to gain understanding. Various methods of calculating the electric field, possible field gradients, along with the molecule's Raman response has provided insight into how confined fields alter the observed signals. ³² Studies have investigated the enhanced molecular response to demonstrate the influence of localized fields. ³³ Other studies have used metallic clusters to model the nanoparticle; ^{22, 34} however, these clusters typically lack the plasmon resonances that are key to many SERS experiments, and still require approximations for the local electric field and dipole re-radiation effects. In light of the chemical effects discussed above, it is important to consider how plasmonic chemical conversion can impact the identity of the molecule being studied and its observed SERS signal.

In the present work we use density functional theory (DFT) and experimental SERS measurements to identify the species detected in SERS measurements from tryptophan (Trp) in gold nanoparticle solutions. Previously we reported that formation of the radical anion resulted in an electronic resonance that gave rise to a surface enhanced resonant Raman scattering (SERRS) effect.²⁹ Using DFT simulations of the vibrational modes and comparing with experiment, we can investigate how the added electron alters the vibrational signal to determine which modes are altered and can serve as indicators of possible radical anion formation. Modulating the environment and altering the chemical structure enables us to investigate the electron localization. Our results show that identifying the correct species enables interpretation of changes in the vibrational spectrum that do not correspond to the closed-shell species in solution. While these chemical effects are specific to the analyte, Trp is a key amino acid and of interest for protein detection and understanding the corresponding biological activity.

Methods:

Materials. L-tryptophan (Trp), *N*-acetyltryptophanamide (NATA), Ce(SO₄)₂, HAuCl₄, sodium citrate, HCl, deuterated water (D₂O), and NaOH were all purchased from Sigma-Aldrich and used as received.

Gold Nanoparticle (AuNP) Synthesis. AuNPs (50 nm) were synthesized using a citrate reduction method. ³⁵ Briefly, HAuCl₄ (0.063 g) was dissolved in 500 mL MilliQ H₂O and heated to boiling while stirring. Then, 7.5 mL of 30 mM sodium citrate was added to the solution, while heating continued, and was stirred for an additional 15 minutes. At this point, the solution developed a red color and then was left stirring until cool.

Instrumentation. Raman measurements were obtained using a Snowy Range Instruments IM-52 benchtop Raman spectrometer with a 638 nm excitation laser. UV-Vis measurements were obtained using VWR UV-1600PC spectrometer. Dynamic Light Scattering was performed using a Zetasizer Nano (Malvern). Nanoparticle tracking analysis was obtained using a Nanosight RS3000 (Malvern).

pH dependence of the SERS Signal. A 10 mM stock solution of either Trp or NATA were diluted to 5mM using a ratio of either 100 mM HCl or 100 mM NaOH to H₂O to create different pH solutions. pH was measured of each solution using a micro-pH probe (Orion™ PerpHecT™ ROSS™ Combination pH micro electrode, Thermo Scientific). AuNPs were concentrated to approximately 4 x10¹⁰ particles/mL by centrifugation at 6000 rpm for 20 mins followed by resuspension in MilliQ H₂O. The particle concentration was measured using nanoparticle tracking analysis. 200uL of the 10 mM analyte solution was added to 200uL of the concentrated AuNPs and the solutions were analyzed on a Snowy Range Spectrometer by averaging 3 acquisitions of 10 s each, with 23 mW laser excitation. Solutions were then added to 600 uL MilliQ H₂O and analyzed with an UV-Vis spectrometer (400-1000 nm) and DLS.

Density-Functional Theory (DFT) Calculations. All calculations were performed with Gaussian 16. ³⁶ The initial geometries of Trp and NATA and the corresponding protonation states were taken from PubCHEM³⁷⁻³⁸ and modified using Gaussview 6.³⁹ Geometry optimizations followed by frequency analyses, including the Raman intensities, were performed using the B3LYP and CAM-B3LYP functionals with the 6-31+G(d) basis set. ⁴⁰⁻⁴³ Optimized stationary points were confirmed to be local minima by examining the resulting vibrational frequencies to make sure all calculated frequencies were real values. Aqueous solvation effects were simulated with the solvation model density (SMD) method with electrostatics in terms of the integral-equation formalism polarizable continuum model (IEF-PCM). ⁴⁴⁻⁴⁶

B3LYP and CAM-B3LYP functionals were utilized for each species with the 6-31+G(d) basis set. The simulated Raman spectra were generated in Gaussview 6 with the default 4 cm⁻¹ linewidth parameter for peak half width at half height (HWHH), which gave a realistic spectrum for Trp. Scaling factors for the simulated Raman spectrum were calculated by matching the corresponding vibrations from the experiment to the simulated spectrum through displacement vector analysis and prior literature assignments.⁴⁷ Differences in the experimental vibrational frequency and the

uncorrected simulated frequency for each mode were used to determine the scaling factor for each simulated spectrum, as well as the root mean square (RMS) error, using the approach of Scott and Radom⁴⁸ (see SI for details). The vibrational frequencies for closed-shell Trp, simulated using both B3LYP and CAM-BL3YP functionals, are shown in **Table S1** with the calculated scaling factors. The vibrational frequencies and determined scaling factors for the radical cation, simulated with both B3LYP and CAM-B3LYP functionals, are shown in **Table S2**. The scaling factors for all species were found to be 0.98 and applied to generate the simulated Raman spectra.

Time Dependent Density Functional Theory (TD-DFT) Calculations. Simulated UV-vis spectra were generated for each system. Single-point TD-DFT calculations were performed for all of the previously optimized conformations (CAM-B3LYP and B3LYP, along with the 6-31+G(d) basis set) with the same solvation model (SMD) with Gaussian 16. Using the simulated UV-vis peaks from the TD-DFT calculation, the simulated spectra were generated in Gaussview 6 with the default (2685.83 cm⁻¹) linewidth parameter, which gave a realistic spectrum for Trp.

Spectral Data Processing. To help visualize the relative changes in the spectra, each SERS spectrum was normalized by subtracting a constant background, such that the lowest intensity value was set to 0, and then dividing by the highest intensity within the spectral range, such that the most intense peak had an intensity value of 1.

Results:

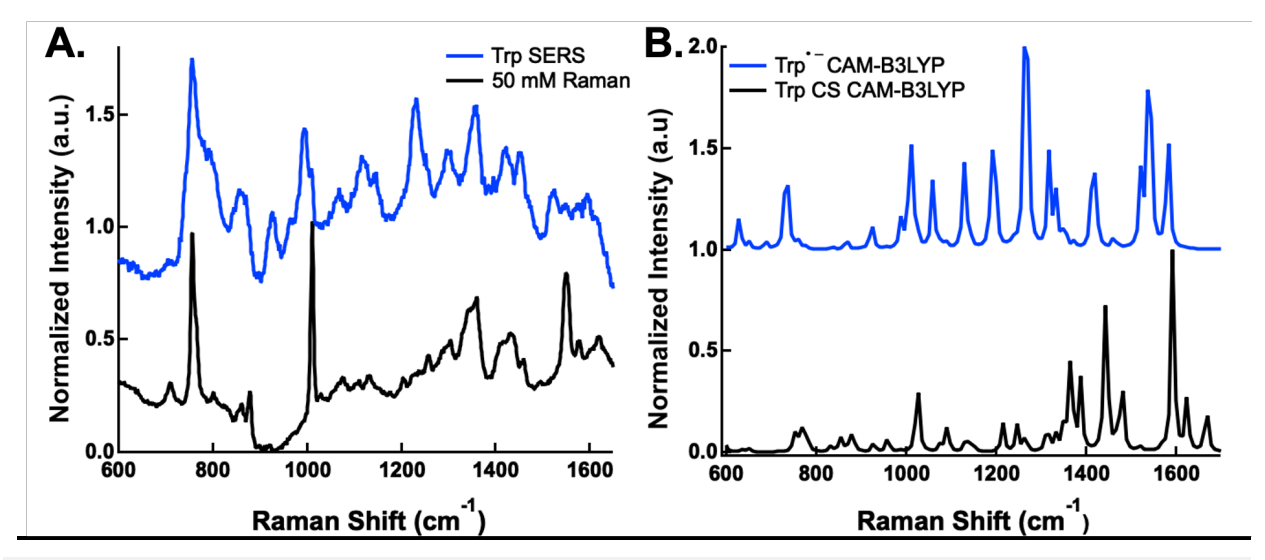


Figure 1: A) The spontaneous Raman spectrum of 50 mM Trp (black) is compared to the SERS spectrum of a AuNP suspension containing 2 mM Trp (blue). B) Simulated Raman spectrum at CAM-B3LYP/6-31+G(d) of the solvated (SMD) closed shell Trp (black) compared to the Trp radical anion (blue). The spectra in both (A) and (B) are normalized and offset for clarity.

Figure 1 shows the experimental SERS spectrum obtained from a solution of Trp with AuNP compared to the spontaneous Raman spectrum of a 50 mM Trp solution, as well as the simulated spectra arising from the solvated closed-shell and radical anion species of tryptophan. In **Figure 1A**, the experimental SERS spectrum shows new peaks observed at 799 cm⁻¹, 927 cm⁻¹, and 1524 cm⁻¹. Other peaks appear to exhibit significant peak shifts from the normal Raman spectrum, such as the peaks seen at 995 cm⁻¹, 1147 cm⁻¹, and 1422 cm⁻¹. The peaks observed in the spontaneous Raman spectrum agree with established literature assignments for Trp (Table 1, **Figure S1**). ⁴⁷ The simulated SERS spectrum for the solvated closed-shell Trp molecule at the CAM-B3LYP (**Table 1**) and B3LYP (**Table S1**) show differences. The B3LYP method has a lower RMS error when compared to the experimental spectrum; however, the CAM-B3LYP level of theory yields a lower RMS error for the radical species (see below). **Figure 1B** shows the spectrum from the CAM-B3LYP to illustrate the changes observed with electron addition within the same level of theory. The simulated spectra offer a molecular level explanation of the changes in the experimentally observed Raman peaks.

Table 1: Experimental, literature, and simulated (B3LYP/6-31+G(d)) vibrational modes for the solvated closed-shell ground state of

Tryptophan

пурюрнан			
Experiment (cm ⁻¹)	Literature (cm ⁻¹)	Literature Assignment ^{47, 49}	Calculation (cm ⁻¹)
712			744.2
757	759	W18 - Indole ring breathing mode ¹	758.7
862			846.2
879	879	W17 - Benzene B12 and N₁H motion	869.4
1012	1012	W16 - Benzene ring- breathing	1010.6
1078			1075.7
1112	1111	W14 - Pyrrole C ₂ H bending mode	1118.2
1134	1127	W13 - Benzene B9b-type CH bend	1127.2
1207	1207	W11 - Benzene B14-type Kekulé mode	1200.0
1259	1259	W9 - CH bend and C ₃ C ₉ stretch	1252.8
1305	1305	W8 - C ₃ C ₉ stretch and N₁H bend	1297.4
1345	1342 doublet	W7 - N₁C ₈ stretch in indole ring	1354.7
1360	1362 doublet	W7 - N₁C ₈ stretch in indole ring	1368.3
1411			1403.1
1434	1435	W6 - N₁C₂C₃ symmetric stretch, N₁H bend, and benzene CH bending	1423.7
1460	1462	W5 - Benzene B19a-type mode	1456.5
1549	1552	W3 - C ₂ C ₃ stretch in pyrrole ring	1554.6
1579	1579	W2 - Benzene B8a-type mode	1628.4

In our previous work,²⁹ continuous excitation of the plasmon resonance increased the intensity of the SERS bands, reproduced here in **Figure 1**, which we attributed to a stable radical anion formed from the transfer of an electron in the excited plasmon resonance of the AuNP to a Trp in close proximity within the Trp-AuNP suspension. The interaction with the AuNP produced an electronic resonance from the suspension consistent with the formation of the Trp radical. To further support this hypothesis, density functional theory (DFT) calculations were performed to simulate the corresponding Raman vibrations.

-

¹ Numerical assignments are provided in the first panel in Figure S1

The closed-shell singlet state of Trp was calculated with the B3LYP functional in water and compared to both the literature of known Trp Raman responses as well as the experimental spontaneous Raman spectrum, as shown in **Figure 2**. The DFT calculated Raman frequencies were corrected with a factor of 0.98, calculated as described in the methods, to correct for anharmonic effects that are not considered with the use of the harmonic oscillator approximation.⁵⁰ The experimental vibrational modes, the uncorrected calculated modes, along with the calculated correction for each mode are shown in **Table S1**. Vibrational assignments were made by matching the displacement factor from the calculation for each vibrational mode to those reported by Harada et al.⁴⁷ The calculated displacement vectors for each vibration are shown in **Figure S1**. **Table 1** lists the experimental frequencies and DFT calculation for each vibrational mode along with the known literature assignment of each band of Trp.

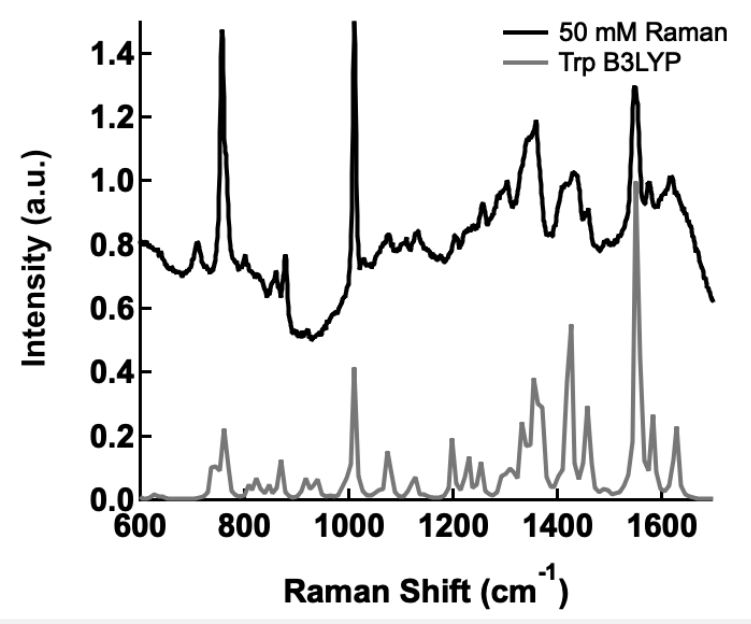


Figure 2: Simulated Raman spectrum for the closed-shell singlet state of Trp at the B3LYP/6-31+G(d) level of theory overlayed with the spontaneous Raman spectrum from a 50 mM Trp solution. The simulated vibrational frequencies are scaled by a factor of 0.98 and include application of a Gaussian broadening function (4 cm⁻¹, HWHH).

In **Figure 2**, the vibrational frequencies of the closed-shell Trp molecule are best represented by the DFT calculations performed at the B3LYP/6-31+G(d) level of theory. The comparison to the DFT calculations performed at the CAM-B3LYP/6-31+G(d) level of theory is shown in **Figure S2**. To address the changes observed in the SERS spectrum (**Figure 1**), we calculated the Raman spectrum expected for the open-shell radical species of Trp.

The Raman spectrum of the radical cation Trp⁺⁺ has been previously reported in the literature and shown to qualitatively agree with the SERS spectrum from a chemical oxidization of Trp with Ce(SO₄)₂. ^{29, 49} To assess the appropriate method for simulating radical species, **Figure S3** plots the comparison between the Raman spectrum calculated using the CAM-B3LYP functional in implicit water for Trp⁺⁺ with the experimental SERS of the species formed through oxidizing Trp with Ce(SO₄)₂. The CAM-B3LYP method adds a correction to the B3LYP method for charge transfer.⁵¹ Indeed, the CAM-B3LYP functional exhibits a lower RMS error than B3LYP for the charged radical species. The comparison of the experimental SERS of Trp⁺⁺ to the simulated Trp⁺⁺ Raman spectrum at the B3LYP method in water (SMD) is shown in **Figure S4**. The frequency scaling factor of 0.98 was determined for the radical cation as described in the methods. **Table S3** lists the frequencies from the SERS experiment, literature, and uncorrected calculation. Slight shifts in the experimental SERS frequencies, relative to the reported literature values, are attributed to modest interaction with the AuNPs. Interestingly, the Trp cation is experimentally observed transiently in solution; however, on the AuNPs the SERS signal of the Trp⁺⁺ is observed to be more stable.

The radical anion species (Trp⁻) was calculated and compared with experimental SERS spectrum of Trp to see how well this model represents the anomalous peaks observed in the Trp experimental SERS spectrum. DFT calculations of Trp⁻ used the CAM-B3LYP functional in implicit water. This comparison is shown in **Figure 3** where the background is subtracted, and the normalized experimental SERS spectrum is plotted along with the normalized calculated spectrum. The comparison of the experimental SERS spectrum to the simulated Raman spectrum at the B3LYP/6-31+G(d) level of theory in implicit water is shown in **Figure S5**. Calculations using more extensive basis sets and additional functionals did not alter the frequencies of the Trp⁻ species (**Figure S6**). The calculated frequencies of Trp⁻ were again corrected using the 0.98 scaling factor determined for Trp and Trp⁺⁺. The comparison of Trp⁻ calculations to the experimental SERS of Trp shows good agreement. In particular, the changes in the simulated spectra of the closed shell and radical anion (**Figure 1**) show good agreement with observed experimental changes in the SERS spectrum (**Table 2**).

Table 2: Experimental and Calculated (CAM-B3LYP/6-31+G(d)) vibrational modes for Trp⁻. The terms used for the assignments are derived from Harada et al.⁴⁷ as noted in Table 1.

SERS Experimental	Trp - Scaled	Matched to Closed-
Frequency (cm ⁻¹)	Calculated	Shell Trp
requeries (em)	Frequency(cm ⁻¹)	Vibrations ^{47, 49} (cm ⁻¹)
	628.8	(0.11)
	650.8	
	687.6	
	733.0	759 (W18)
	738.3	
758	757.8	
799	773.7	
	836.7	
858	867.0	879 (W17)
870	897.8	,
927	922.7	
	956.8	
995	988.6	1012 (W16)
1010	1009.2	ì
	1022.4	
1068	1059.2	
	1074.5	
	1086.9	
1118	1128.3	1111 (W14)
1147	1139.9	1127 (W13)
	1184.6	
	1194.9	
1233	1237.0	
	1266.0	
1303	1317.6	1305 (W8)
	1332.9	
1358	1348.7	1362 (W7)
	1354.5	
	1372.7	
	1411.6	
1422	1420.4	
	1432.3	
1454	1459.8	
	1466.9	
	1474.2	
1524	1522.4	
1549	1540.2	1552 (W3)
	1565.8	
	1581.6	
	1593.1	
	1621.3	

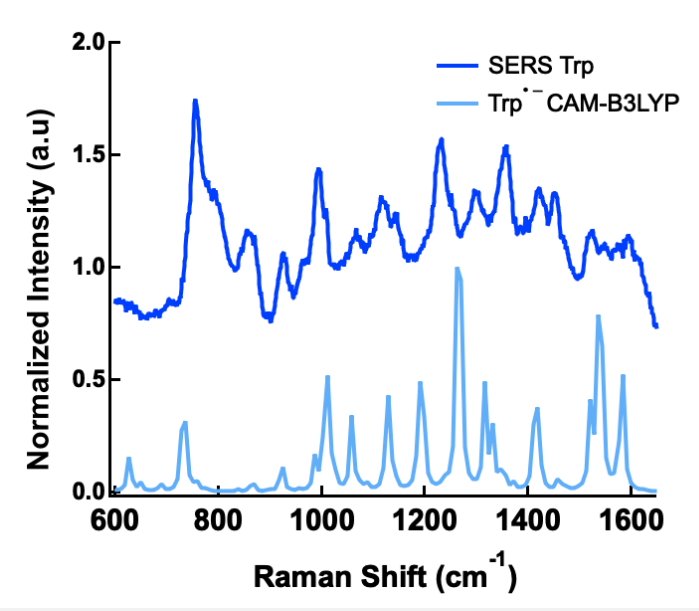


Figure 3: Simulated Raman spectrum for Trp at the CAM-B3LYP/6-31+G(d) level of theory with an applied scaling factor of 0.98 and application of a Gaussian broadening function (4 cm⁻¹, HWHH), while compared to the experimental SERS spectrum of Trp.

To further explore the molecular origins of the anomalous SERS peaks, we compared the simulated vibrational displacement of Trp modes with the known modes of Trp. This analysis consisted of correlating the displacement vectors of the known Trp bands with the prior literature assignments, provided by Harada et al. and matched to the simulated close shell displacement vectors reported herein. Comparison of Trp with the known vibrational modes of close shell Trp indicates agreement for the modes assigned to W18, W17, W13, W8, W7, and W3. These specific bands are indicated in Table 2 with the known literature assignments. The simulated displacement vector images are provided in **Figure S7**. Of note, the bands consistent with closed-shell Trp largely consist of motion associated with the hydrogens bound to the indole ring. The remaining modes in Table 2 show unique displacement vectors (**Figure S7**), suggestive of deformation in the indole ring moiety itself.

Interestingly, varying the Trp concentration in the suspension results in disproportionate changes in the SERS spectrum at 1010 cm⁻¹ (**Figure S8A**). The intensity of the band at 1010 cm⁻¹ changes more dramatically than other features in the spectrum. At 10 mM, the band at 1010 cm⁻¹ is more intense than the adjacent band at 995 cm⁻¹, but at 2 mM, the 1010 cm⁻¹ band is observed as a subtle shoulder on the 995 cm⁻¹ band. The spontaneous Raman limit of detection in this

experimental configuration is calculated to be approximately 5 mM (**Figure S8B**); however, the intensity observed at the given concentrations suggests some degree of closed-shell Trp is also observed in the SERS spectrum. The presence of both the closed-shell and the new species may indicate some form of an aggregate is involved in stabilizing the captured electron.

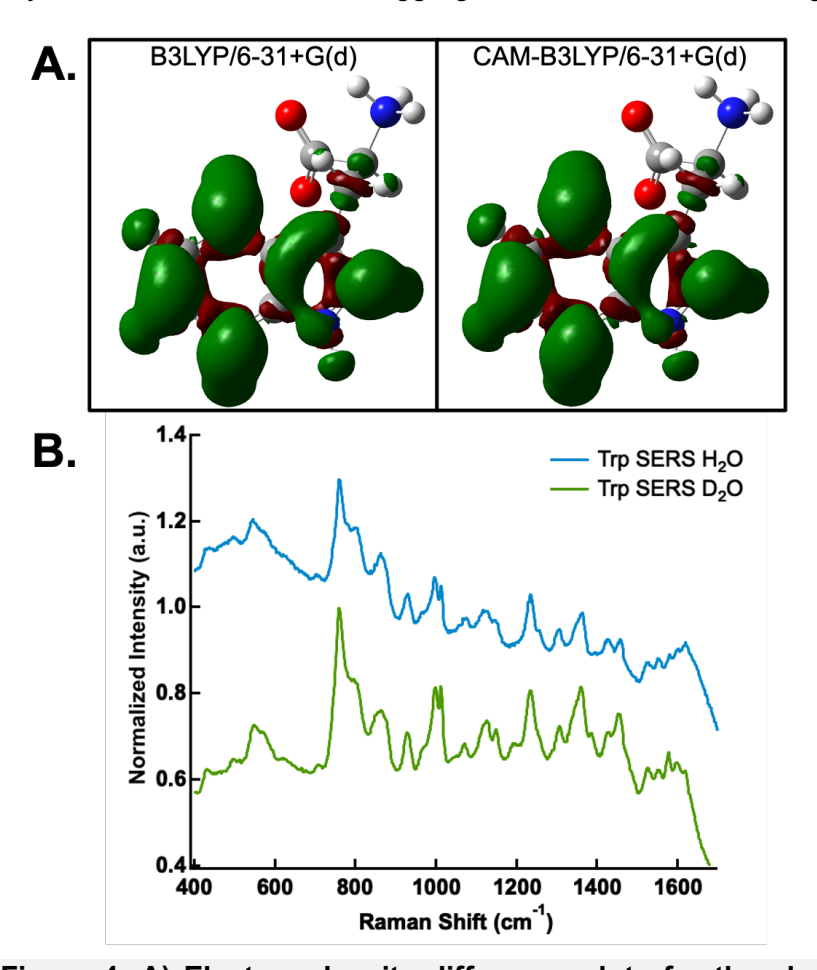


Figure 4: A) Electron density difference plots for the closed-shell singlet (S_0) ground state of Trp being subtracted from that of the radical anion of Trp are shown at both the B3LYP/6-31+G(d) and CAM-B3LYP/6-31+G(d) levels of theory, using the geometry of the S_0 ground state for each respective method. For the electron density difference plots, green indicates a positive value where the radical anion has greater electron density and red indicates a negative value where the closed-shell singlet (S_0) state has greater electron density (using an isovalue contour of 0.001 au). B) The Trp SERS spectra obtained from D_2O (green) and H_2O (blue) solutions show agreement in the peaks observed.

Figure 4A shows electron density difference plots generated by subtracting the electron density of the ground electronic state of the closed-shell singlet from the electron density of the radical

anion (and at the same geometry of the S_0 ground state). The radical anion shows additional electron density in the ring structure at both levels of theory investigated, supporting the localization of the captured electron to this moiety in agreement with the distorted vibrational modes. To further test this hypothesis, we dissolved Trp in D_2O and combined with our AuNP into suspension at a 4:1 (Trp in D_2O : AuNP) volumetric ratio. **Figure 4B** shows the observed SERS spectra in D_2O compared with the result from H_2O . All major peaks are observed at the same frequency, with some low intensity peaks changing (e.g. 1195 and 1385 cm⁻¹ appears in the D_2O spectrum). The D_2O spectrum also shows a decrease in intensity above 1600 cm⁻¹ Raman shift, likely arising from a lower spontaneous Raman background from the solvent. The significant agreement of all the major features in the Trp SERS spectrum indicates the shifts do not arise from hydrogen bonding, but rather agrees with the hypothesized change in the electronic configuration.

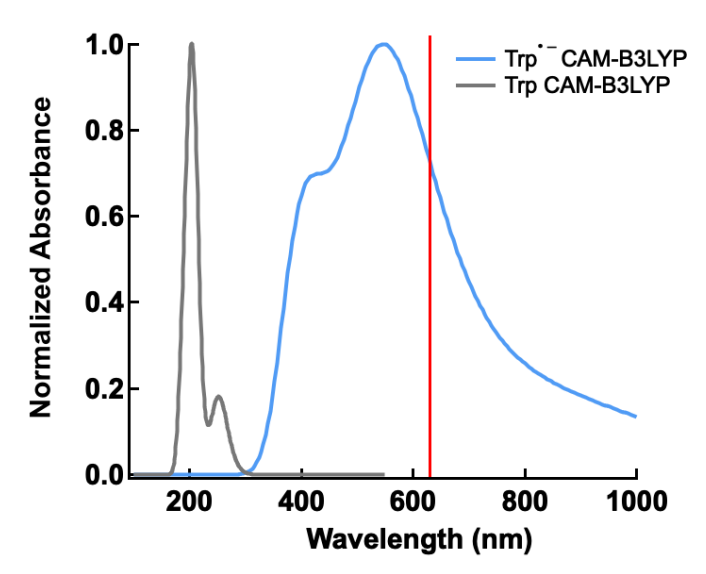


Figure 5: Simulated UV-vis spectra for the closedshell singlet state of Trp at the CAM-B3LYP/6-31+G(d) level of theory (grey) compared to that of Trp' (blue). The red line indicates a 638 nm excitation wavelength for SERS enhancement.

Figure 5 shows the calculated UV-vis spectra obtained using time-dependent density functional theory (TD-DFT) with the CAM-B3LYP/6-31+G(d) model for the solvated radical anion and closed-shell species. In our prior work, the gas-phase calculation showed a resonance that agreed with an absorption band observed in the UV-Vis extinction spectrum.²⁹ Here, adding solvation to the model further shifts the resonance to longer wavelengths and in better agreement

with the experiment. The simulation supports a selective enhancement of the SERS peaks specific to Trp* by showing a change in the absorbance spectrum compared to the calculated spectrum for closed-shell singlet state of Trp. The absorbance of Trp* near 600 nm overlaps with the 638 nm laser used for the SERS measurement. The overlap between the excitation laser wavelength and the Trp* absorbance suggests that Trp* experiences a resonance Raman enhancement in addition to the SERS enhancement. The excitation wavelength used to obtain the SERS spectrum reported in **Figure 1** and **Figure 3** is indicated in **Figure 5** using a red line. In resonance Raman, the observed vibrational frequencies arise from the ground state species. The Trp SERS spectra observed are consistent with the simulated spectrum of the ground state radical anion, indicating electron transfer occurs prior to the Raman excitation.

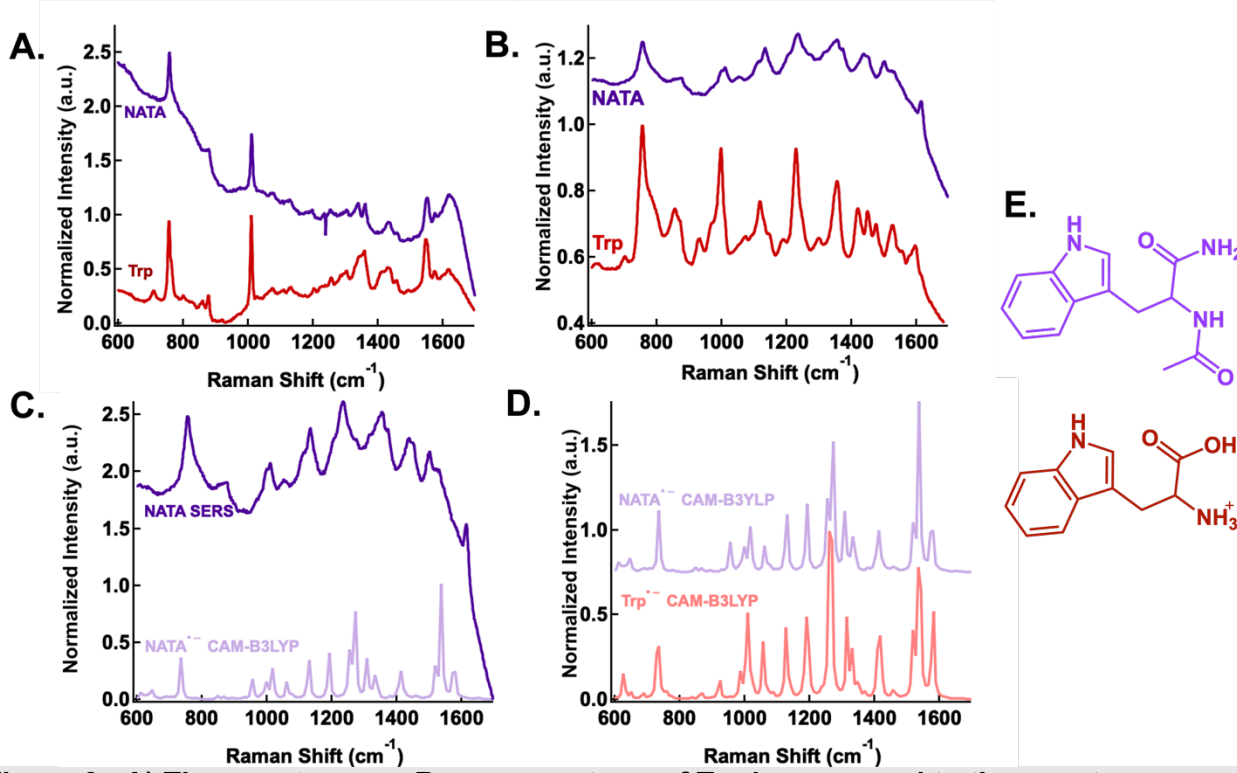


Figure 6: A) The spontaneous Raman spectrum of Trp is compared to the spontaneous Raman spectrum of NATA. B) Comparison of SERS spectra of NATA and Trp at equivalent pH values. C) NATA SERS compared to the simulated Raman spectrum at the CAM-B3LYP/6-31+G(d) level of theory (with SMD implicit water) for NATA⁻. D) Comparison of the simulated Raman spectrum at the CAM-B3LYP/6-31+G(d) level of theory and solvation (SMD) for Trp⁻ and NATA⁻. E) The structure of NATA (purple) and Trp (red) structures are shown. All calculated vibrational frequencies have been scaled by 0.98 and a 4 cm⁻¹ Gaussian broadening has been applied.

Our experiments on tryptophan support the observed SERS signals arise from the ground state radical anion, and further suggest the captured electron is localized to the indole moiety. *N*-acetyltryptophanamide (NATA) is often used in comparison to Trp because it contains the same indole ring moiety. ⁴⁹ Modifications were made to the amino acid backbone through acetylation of the amino group and amidation of the carboxylic acid. Due to the similar structures of NATA and Trp, the normal Raman spectra do not vary significantly as shown in **Figure 6A**. **Figure 6B** shows the observed SERS spectrum of NATA compared to that of Trp, which also strongly resemble one another. It is worth noting that the SERS spectrum of NATA was obtained at an acidic pH so the comparison shown in **Figure 6B** is of Trp at an equivalent pH value. The Raman spectrum of radical anion of NATA (NATA⁻⁻) was calculated and compared to the NATA SERS spectrum, shown in **Figure 6C**, as well as the calculated Raman spectrum of Trp'-, shown in **Figure 6D**. Both calculated spectra have the 0.98 correction previously established applied to the vibrational frequencies. Again we observe agreement between the SERS spectra and the calculated spectra of NATA⁻⁻ and Trp'-, providing further support that the electron is stabilized within the indole ring of both molecules.

Table S4 shows the SERS experimental peaks for NATA along with the vibrational assignments and the calculated values for NATA*. In **Table S4**, the experimental SERS spectrum of NATA shows two bands that correlate with W14. The experimental band at 1053 cm⁻¹ is slightly shifted from the spontaneous Raman spectrum frequency of 1078 cm⁻¹. There is also a second band in the NATA SERS spectrum at 1112 cm⁻¹, indicated in the table with *, which could also correspond with W14 and occurs at similar frequency as observed with Trp. Vibrational analysis of the calculated NATA*—was performed to assess if NATA experiences similar vibrational distortions to Trp with the addition of an electron. The NATA calculations show the same distorted vibrations observed with the calculated Trp*—. The similar simulated vibrations and observed SERS spectra suggest a consistent stabilization of the electron within the indole ring for both NATA and Trp.

The pH dependence on the SERS spectra of NATA suggest changes in pH may alter the electron-transfer process. **Figure S9** shows that no significant changes to the normal Raman spectrum are observed with varying the pH of the Trp solution. The simulated Raman spectra with the B3LYP functional in implicit water under varying pH conditions also show minimal changes in the Raman spectrum at different pH values.

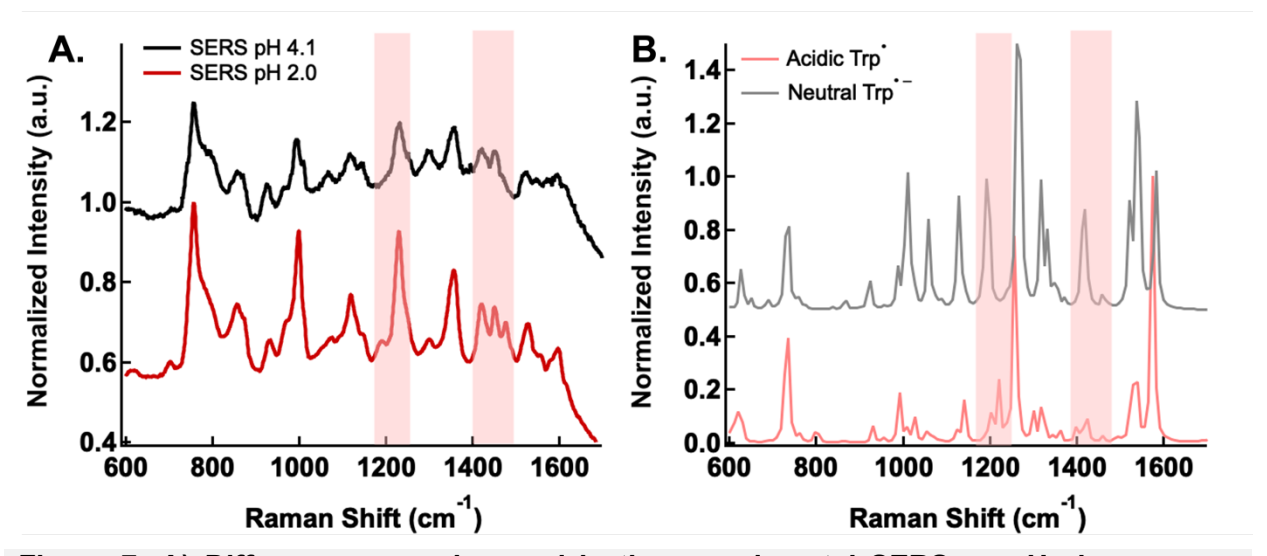


Figure 7: A) Differences are observed in the experimental SERS as pH changes are highlighted with red boxes and the B) simulated Raman spectra at the CAM-B3LYP/6-31+G(d) level of theory for the Trp radical (Trp') species at an acidic pH value and the Trp radical anion (Trp') at neutral pH values. For convenience, the changes are highlighted with red shading. Calculated vibrational frequencies have been scaled by 0.98 and a 4 cm⁻¹ Gaussian broadening has been applied.

Figure 7 shows the comparison of the Trp SERS at pH 2 (red) and pH 4 (black), where the assynthesized AuNP solutions were slightly acidic and resulted in a pH of 4. An acidic pH appears to be necessary for the formation of the radical anion species. **Figure S10A** shows the pH of the Trp solution is important for observing the SERS spectrum. The pH dependence of NATA was also tested and showed a similar dependence on pH as Trp (**Figure S10B**).

Figure 7A shows some notable changes near 1200 and 1400 cm⁻¹ when the solution is made more acidic from pH 4 to pH 2. Both the experimental and calculated spectra show consistent changes in the spectrum at 1230 cm⁻¹, 1422 cm⁻¹, and 1454 cm⁻¹. Specifically, at pH 2, the experimental Trp spectrum shows a shoulder near 1191 cm⁻¹ and an additional peak at 1477 cm⁻¹. These differences are likely the result of the change in protonation state of the radical anion with a more acidic pH, consistent with the p K_a of 2.4 for the backbone of Trp. **Figure S11** shows the species expected at varying pH, based on the p K_a values of Trp.³⁷

The calculated Raman spectrum of the radical anion at neutral pH has a peak at 1230 cm⁻¹ corresponding to the experimentally observed peak at 1237 cm⁻¹ as shown in **Figure 7B**. The Trp spectrum at a pH of 2 shows a shoulder on the peak observed at 1220 cm⁻¹ that is also observed in the calculated spectrum at equivalent pH. Furthermore, the changes in the spectrum observed

near 1400 cm⁻¹ are also consistent with the calculated spectra at different pH values. Raman bands for the radical anion at neutral pH are observed experimentally at 1422 and 1454 cm⁻¹ calculated at 1420.4 and 1459.8 cm⁻¹, respectively. At pH values below the p K_a , a third band is observed in both the experimental SERS spectrum and calculated Trp⁻ Raman spectrum. In addition to the changes in the Raman spectra, TD-DFT calculations (**Figure S12**) show electronic transitions of Trp radical at neutral and acidic pH near the 638 nm excitation wavelength used in the SERS experiment.

Trp and NATA show negligible SERS signals at pH 6 and higher. The change in the SERS signal at pH 6 correlates with a change in protonation state of the citrate capping agent on the AuNPs. Sodium citrate tribasic dihydrate has p K_a values of 3.18, 4.76, and 6.40. ⁵² By changing the protonation state of the citrate at pH 4, Trp can more easily displace the citrate and interact more directly with the surface of the AuNP, hence an increase in the SERS signal. It is reported that both amine and carboxylic acid groups have a pH dependent affinity for binding to Au surfaces both of which are present in Trp and NATA. ⁵³⁻⁵⁵

Discussion:

Our results support the hypothesis that electron-transfer processes alter the observed Raman frequencies detected in SERS experiments. This has consequences on the assignment and interpretation of SERS spectra as well as chemical conversion processes that occur on the surface of nanoparticles.

Traditionally, peak assignments in a SERS spectrum are based on the vibrational frequencies observed in the spontaneous Raman spectrum. For proteins, these signals are associated with the amino acids that comprise them. ⁵⁶⁻⁵⁸ It has been previously reported that SERS spectra of peptides and proteins mostly contain peaks associated with aromatic amino acid, such as tryptophan, tyrosine, and phenylalanine, due to their larger Raman cross sections. ^{18-19, 59} The known spontaneous Raman signals of these amino acids have been utilized for the SERS detection of proteins. Our work suggests that basing the SERS assignments solely on the spontaneous Raman spectrum of these amino acids, specifically tryptophan (Trp), does not give an entirely accurate description for the origins of the band assignments associated with the amino acids in the SERS spectra.

The SERS of Trp obtained in colloidal suspension of gold nanoparticles (AuNP) results in a spectrum that has many differences from the spontaneous Raman spectrum obtained from Trp, as shown in Figure 1A. Others have reported a similar SERS spectrum form Trp on gold nanoparticles. In the absence of experiments to assess aggregation, they attributed changes in the UV-Vis spectrum to nanoparticle coupling, and the changes in the SERS spectrum are attributed to adsorptive interactions.^{28, 60} In our previous paper we performed dynamic light scattering with UV-Vis absorption to demonstrate the nanoparticles were unaggregated and the new resonance was associated with the presence of tryptophan.²⁹ This supported assigning the new SERS peaks and peak shifts to corresponding bands in the simulated Raman spectrum for the Trp radical anion (Trp*-) species.²⁹ The calculated Trp*- Raman spectrum, shown in **Figure 3**, accounts for the differences observed between the SERS and the normal Raman spectrum of Trp. We associate these differences with shifts in energy and distortions of vibrational modes from DFT calculations of Trp' (Figure 4). The calculations indicate vibrational mode distortions in the radical anion that are localized within the indole ring sidechain of Trp*. These Trp SERS peaks at 1010, 1118, 927, and 1454 cm⁻¹ are also observed in the SERS spectrum of the Trp-cage protein.²⁹ Using assignments based on the normal Raman spectra of amino acids, these shifted bands suggest the SERS community could be missing signatures of Trp residues when studying SERS of proteins. Indeed, the additional resonance enhancement shown, generating a SERRS effect (Figure 5), suggests the peaks observed are likely dominated by Trp⁻ and potentially other electron-transfer products.

The presence of Trp⁻⁻ was unexpected. The Trp radical cation (Trp⁻⁺) is commonly reported in the protein literature, where Trp serves as an electron donor. ^{49, 60-65} Indeed, others have used NATA alongside Trp to study the radical cation due to their similarities in structure and the ability to associate changes with the indole ring moiety. The similarities in the SERS spectrum of Trp and NATA confirm that the signal obtained results from the indole ring structure. The vibrational modes calculated for Trp⁻⁻ and NATA⁻⁻ indicate the additional electron is localized in the indole ring for both NATA and Trp, where the same vibrational mode distortions are observed in the calculated spectra of the Trp⁻⁻ and NATA⁻⁻ shown in **Figure 6**. This localization is additionally supported with the electron density difference plots shown in **Figure 4A**. Interestingly, the formation of the radical anion (or electron capture) is consistent with recent results reported by Zenobi et al.^{14, 66} In prior studies, the capture of a hot electron from a tip-enhanced Raman experiment (TERS) on peptides results in bond cleavage. The indole ring of Trp appears to

stabilize the additional electron without cleavage. It is worth noting the peptides studied by Zenobi et al. did not contain Trp residues.

Our work indicates electron transfer impacts the observed spectrum and, if a resonant electronic state forms, can provide additional chemical enhancement. Habteyes et al. has summarized various explanations of a plasmon-induced charge-transfer compared to hot-electron driven chemistry. ⁸ The SERS literature has long recognized that charge-transfer states can form from molecules adsorbed to the metal surface. ^{9, 67-73} While some shifts occur due to adsorption, the vibrations observed still correspond the ground state of the adsorbed species. The observed SERS intensities are altered by the Frank-Condon overlap between the ground and accessed excited electronic state. The agreement of the observe frequencies between the experimental SERS spectrum and the calculated Raman spectrum of the Trp* indicates the ground state radical anion is the species that gives rise to the observed signal. ¹⁴

Indeed, other reports have shown that electron transfer, or molecular charging to form a radical anion, can affect the observed Raman response. ⁷⁴ The agreement between the experimental SERS and calculated Raman of Trp⁻⁻ suggests that plasmon-driven, hot electrons are forming Trp⁻⁻. Van Duyne et al. studied the formation of the radical anion of *trans*-1,2-*bis*-(4-pyridyl)ethylene (BPE), after pumping with a 532 nm laser and probing with a 785 nm laser. They observe variations in their SERS spectra that are associated with the radical anion of BPE. ¹⁵⁻¹⁶ Our previous work also shows the ability to pump hot electrons with a 532 nm excitation and observe increased intensity associated with Trp⁻⁻ formation. ²⁹

Our explanation of a stable radical due to hot-electron transfer remain consistent when the pH is modified in the experimental solution and the protonation state is modified in the calculated species based on the p K_a of Trp (**Figure 7**). Prior reports have suggested lower pH increases the interaction of Trp with citrate reduced AuNPs.²⁸ There are some distinct differences in the experimental SERS spectra at pH 4 and pH 2 which we have shown can be calculated and correlated with the ground state of each species under the corresponding protonation state, or pH. Interestingly, the pH dependence suggests additional factors impact the formation of Trp $^-$. Haes et al. show the impact of pH on intermolecular interactions, which in turn impact the SERS signal of small molecules such as mercaptobenzoic acid (MBA). ⁵³ When the experimental pH is adjusted to 6, the signals from Trp $^-$ and NATA $^-$ decrease (**Figure S10**). This is not a pH associated with p K_a values of Trp but rather the p K_a values of the citrate that caps the AuNP.

When the protonation state of citrate is changed, the Trp or NATA can more easily displace the citrate interacting more readily with the AuNP. ^{54, 75-78} Alternatively, rather than impacting the proximity of the Trp to the surface, the citrate may more readily accept the energetic electron, effectively shielding the Trp from the electron-transfer process. Additional work is needed to understand how competing molecules affect the observed SERS signals. It appears important to consider everything in solution that can impact the transfer of a hot electron, which may impact our understanding of hot-electron transfer relevant to chemical sensing but also catalysis and chemical conversion using plasmonic materials.

Conclusion:

The combination of experiment and DFT calculations show that electron capture by the indole ring of tryptophan (Trp), and other indole containing molecules (such as, NATA) give rise to changes in the observed SERS spectrum. DFT calculations indicate the frequency changes are consistent with a ground state radical anion species being detected (Trp'- and NATA'-). The vibrational frequencies calculated for Trp'- show changes with pH consistent with the experimental SERS spectrum, further indicating the radical anion structure is consistent with the detected signal. Interestingly, competition with other surface adsorbates, such as citrate, appears to regulate the formation of the radical anion. Additional experiments are needed to assess the intermolecular interactions and possible molecular aggregates on the observed SERS signal. Plasmonic driven chemistries, such as radical formation, are becoming an important in diverse areas of research and improved understanding will enable future applications. By identifying the molecular identity of analytes, DFT calculations can be more readily applied to interpret the enhanced Raman signals observed in SERS experiments.

Acknowledgment. The authors acknowledge support from the National Science Foundation Award CHE-2107791 and The Ohio State University. Generous computational resources were provided by the Ohio Supercomputer Center.

Supporting Information Available: Supporting Figures S1-S12 are provided, showing additional experimental and calculated results; Tables S1-S4 tabulating the experimental, calculated, and literature vibrational frequencies for the closed-shell ground state of Trp and the Trp radical cation; details of how the scaling factors were derived; and the coordinates for the optimized structures used in our calculations.

References.

- 1. Stiles, P. L.; Dieringer, J. A.; Shah, N. C.; Van Duyne, R. P., Surface-Enhanced Raman Spectroscopy. *Annual Review of Analytical Chemistry* **2008**, *1*, 601-626.
- 2. McNay, G., Eustace, David, Smith, Ewen, W., Faulds, Karen, Graham, Duncan, Surface-Enhanced Raman Scattering (Sers) and Surface-Enhanced Resonance Raman Scattering (Serrs): A Review of Applications. *Appl. Spectrosc.* **2011**, *65*, 825-837.
- 3. Albrecht, M. G.; Creighton, J. A., Anomalously Intense Raman Spectra of Pyridine at a Silver Electrode. *Journal of the American Chemical Society* **2002**, *99*, 5215-5217.
- 4. Van Duyne, R. P., Raman Applications of Raman Spectroscopy in Electrochemistry. *Le Journal de Physique Colloques* **1977**, *38*, C5-239-C5-252.
- 5. Langer, J.; Jimenez de Aberasturi, D.; Aizpurua, J.; Alvarez-Puebla, R. A.; Auguié, B.; Baumberg, J. J.; Bazan, G. C.; Bell, S. E. J.; Boisen, A.; Brolo, A. G., et al., Present and Future of Surface-Enhanced Raman Scattering. *ACS Nano* **2019**, *14*, 28-117.
- 6. Willets, K. A.; Van Duyne, R. P., Localized Surface Plasmon Resonance Spectroscopy and Sensing. *Annual Review of Physical Chemistry* **2007**, *58*, 267-297.
- 7. Lombardi, J. R.; Birke, R. L., A Unified View of Surface-Enhanced Raman Scattering. *Accounts of Chemical Research* **2009**, *42*, 734-742.
- 8. Tesema, T. E.; Kafle, B.; Habteyes, T. G., Plasmon-Driven Reaction Mechanisms: Hot Electron Transfer Versus Plasmon-Pumped Adsorbate Excitation. *The Journal of Physical Chemistry C* **2019**, *123*, 8469-8483.
- 9. Otto, A., The 'Chemical' (Electronic) Contribution to Surface-Enhanced Raman Scattering. *Journal of Raman Spectroscopy* **2005**, *36*, 497-509.
- 10. Kameche, F.; Heni, W.; Telitel, S.; Vidal, L.; Marguet, S.; Douillard, L.; Fiorini-Debuisschert, C.; Bachelot, R.; Soppera, O., Probing Plasmon-Induced Chemical Mechanisms by Free-Radical Nanophotopolymerization. *The Journal of Physical Chemistry C* **2021**, *125*, 8719-8731.
- 11. Kim, M.; Lin, M.; Son, J.; Xu, H.; Nam, J.-M., Hot-Electron-Mediated Photochemical Reactions: Principles, Recent Advances, and Challenges. *Advanced Optical Materials* **2017**, *5*, 1700004.
- 12. Huang, Y.-F.; Zhu, H.-P.; Liu, G.-K.; Wu, D.-Y.; Ren, B.; Tian, Z.-Q., When the Signal Is Not from the Original Molecule to Be Detected: Chemical Transformation of Para-Aminothiophenol on Ag During the Sers Measurement. *Journal of the American Chemical Society* **2010**, *132*, 9244-9246.
- 13. Fang, Y.; Li, Y.; Xu, H.; Sun, M., Ascertaining P,P'-Dimercaptoazobenzene Produced from P-Aminothiophenol by Selective Catalytic Coupling Reaction on Silver Nanoparticles. *Langmuir* **2010**, *26*, 7737-7746.
- 14. Szczerbiński, J.; Gyr, L.; Kaeslin, J.; Zenobi, R., Plasmon-Driven Photocatalysis Leads to Products Known from E-Beam and X-Ray-Induced Surface Chemistry. *Nano Letters* **2018**, *18*, 6740-6749.
- 15. Sprague-Klein, E. A.; McAnally, M. O.; Zhdanov, D. V.; Zrimsek, A. B.; Apkarian, V. A.; Seideman, T.; Schatz, G. C.; Van Duyne, R. P., Observation of Single Molecule Plasmon-Driven Electron Transfer in Isotopically Edited 4,4'-Bipyridine Gold Nanosphere Oligomers. *Journal of the American Chemical Society* **2017**, *139*, 15212-15221.
- 16. Sprague-Klein, E. A.; Negru, B.; Madison, L. R.; Coste, S. C.; Rugg, B. K.; Felts, A. M.; McAnally, M. O.; Banik, M.; Apkarian, V. A.; Wasielewski, M. R., et al., Photoinduced Plasmon-Driven Chemistry in Trans-1,2-Bis(4-Pyridyl)Ethylene Gold Nanosphere Oligomers. *Journal of the American Chemical Society* **2018**, *140*, 10583-10592.
- 17. Huang, Y.-F.; Wang, W.; Guo, H.-Y.; Zhan, C.; Duan, S.; Zhan, D.; Wu, D.-Y.; Ren, B.; Tian, Z.-Q., Microphotoelectrochemical Surface-Enhanced Raman Spectroscopy: Toward

- Bridging Hot-Electron Transfer with a Molecular Reaction. *Journal of the American Chemical Society* **2020**, *142*, 8483-8489.
- 18. Wei, F.; Zhang, D.; Halas, N. J.; Hartgerink, J. D., Aromatic Amino Acids Providing Characteristic Motifs in the Raman and Sers Spectroscopy of Peptides. *The Journal of Physical Chemistry B* **2008**, *112*, 9158-9164.
- 19. Blum, C.; Schmid, T.; Opilik, L.; Metanis, N.; Weidmann, S.; Zenobi, R., Missing Amide I Mode in Gap-Mode Tip-Enhanced Raman Spectra of Proteins. *The Journal of Physical Chemistry C* **2012**, *116*, 23061-23066.
- 20. Wei, F.; Zhang, D.; Halas, N. J.; Hartgerink, J. D., Aromatic Amino Acids Providing Characteristic Motifs in the Raman and Sers Spectroscopy of Peptides. *The journal of physical chemistry. B* **2008**, *112*, 9158-64.
- 21. Kurouski, D.; Postiglione, T.; Deckert-Gaudig, T.; Deckert, V.; Lednev, I. K., Amide I Vibrational Mode Suppression in Surface (Sers) and Tip (Ters) Enhanced Raman Spectra of Protein Specimens. *Analyst* **2013**, *138*, 1665-1673.
- 22. Królikowska, A.; Cukras, J.; Witkowski, M.; Tymecka, D.; Hernik-Magoń, A.; Misicka, A.; Dzwolak, W., Sers and Dft Study of Noble-Metal-Anchored Cys-Trp/Trp-Cys Dipeptides: Influence of Main-Chain Direction and Terminal Modifications. *The Journal of Physical Chemistry C* **2020**, *124*, 7097-7116.
- 23. Podstawka, E.; Proniewicz, L. M., The Orientation of Bn-Related Peptides Adsorbed on Sers-Active Silver Nanoparticles: Comparison with a Silver Electrode Surface. *The Journal of Physical Chemistry B* **2009**, *113*, 4978-4985.
- 24. Podstawka-Proniewicz, E.; Niaura, G.; Proniewicz, L. M., Neuromedin C: Potential-Dependent Surface-Enhanced Raman Spectra in the Far-Red Spectral Region on Silver, Gold, and Copper Surfaces. *The Journal of Physical Chemistry B* **2010**, *114*, 5117-5124.
- 25. Feliu, N.; Hassan, M.; Garcia Rico, E.; Cui, D.; Parak, W.; Alvarez-Puebla, R., Sers Quantification and Characterization of Proteins and Other Biomolecules. *Langmuir* **2017**, *33*, 9711-9730.
- 26. Tu, Q. E., Jonathan; Chang, Chang, Surface-Enhanced Raman Spectroscopy Study of Indolic Molecules Adsorbed on Gold Colloids. *Journal of Biomedical Optics* **2010**, *15*, 020512.
- 27. Joshi, P.; Shewale, V.; Pandey, R.; Shanker, V.; Hussain, S.; Karna, S. P., Tryptophan–Gold Nanoparticle Interaction: A First-Principles Quantum Mechanical Study. *The Journal of Physical Chemistry C* **2011**, *115*, 22818-22826.
- 28. daFonseca, B. G.; Costa, L. A. S.; Sant'Ana, A. C., Insights of Adsorption Mechanisms of Trp-Peptides on Plasmonic Surfaces by Sers. *Spectrochimica Acta Part A: Molecular and Biomolecular Spectroscopy* **2018**, *190*, 383-391.
- 29. Sloan-Dennison, S.; Zoltowski, C. M.; El-Khoury, P. Z.; Schultz, Z. D., Surface Enhanced Raman Scattering Selectivity in Proteins Arises from Electron Capture and Resonant Enhancement of Radical Species. *The Journal of Physical Chemistry C* **2020**, *124*, 9548-9558.
- 30. Cañamares, M. V.; Chenal, C.; Birke, R. L.; Lombardi, J. R., Dft, Sers, and Single-Molecule Sers of Crystal Violet. *The Journal of Physical Chemistry C* **2008**, *112*, 20295-20300.
- 31. Chandra, S.; Chowdhury, J.; Ghosh, M.; Talapatra, G. B., Genesis of Enhanced Raman Bands in Sers Spectra of 2-Mercaptoimidazole: Ftir, Raman, Dft, and Sers. *The Journal of Physical Chemistry A* **2012**, *116*, 10934-10947.
- 32. Payton, J. L.; Morton, S. M.; Moore, J. E.; Jensen, L., A Hybrid Atomistic Electrodynamics-Quantum Mechanical Approach for Simulating Surface-Enhanced Raman Scattering. *Acc Chem Res* **2014**, *47*, 88-99.
- 33. Sonntag, M. D.; Chulhai, D.; Seideman, T.; Jensen, L.; Van Duyne, R. P., The Origin of Relative Intensity Fluctuations in Single-Molecule Tip-Enhanced Raman Spectroscopy. *J. Am. Chem. Soc.* **2013**, *135*, 17187-17192.
- 34. Rodriguez, R. D.; Villagómez, C. J.; Khodadadi, A.; Kupfer, S.; Averkiev, A.; Dedelaite, L.; Tang, F.; Khaywah, M. Y.; Kolchuzhin, V.; Ramanavicius, A., et al., Chemical Enhancement

- Vs Molecule–Substrate Geometry in Plasmon-Enhanced Spectroscopy. *ACS Photonics* **2021**, 8, 2243-2255.
- 35. Frens, G., Controlled Nucleation for the Regulation of the Particle Size in Monodisperse Gold Suspensions. *Nature Physical Science* **1973**, *241*, 20-22.
- 36. Frisch, M. J. T., G.W.; Schlegel, H.B.; Scuseria, G.E.; Robb, M.A.; Cheeseman, J.R.; Scalmani, G.; Barone, V.; Petersson, G.A.; Nakatsuji, H.; et al., Gaussian 16, Revision C.01. *Gaussian. Inc.*
- 37. PubChem, https://pubchem.ncbi.nlm.nih.gov/compound/Tryptophan (accessed August 2, 2021).
- 38. PubChem, https://pubchem.ncbi.nlm.nih.gov/compound/N-Acetyl-L-tryptophanamide (accessed August 2, 2021).
- 39. Dennington, R. K., Todd A.; Millam, John M. *Gaussview*, Version 6; Semichem Inc.: Shawnee Mission, KS, 2016.
- 40. Clark, T.; Chandrasekhar, J.; Spitznagel, G. n. W.; Schleyer, P. V. R., Efficient Diffuse Function-Augmented Basis Sets for Anion Calculations. lii. The 3-21+G Basis Set for First-Row Elements, Li-F. *Journal of Computational Chemistry* **1983**, *4*, 294-301.
- 41. Ditchfield, R.; Hehre, W. J.; Pople, J. A., Self-Consistent Molecular-Orbital Methods. Ix. An Extended Gaussian-Type Basis for Molecular-Orbital Studies of Organic Molecules. *The Journal of Chemical Physics* **1971**, *54*, 724-728.
- 42. Hariharan, P. C.; Pople, J. A., The Influence of Polarization Functions on Molecular Orbital Hydrogenation Energies. *Theoretica Chimica Acta* **1973**, *28*, 213-222.
- 43. Hehre, W. J.; Ditchfield, R.; Pople, J. A., Self—Consistent Molecular Orbital Methods. Xii. Further Extensions of Gaussian—Type Basis Sets for Use in Molecular Orbital Studies of Organic Molecules. *The Journal of Chemical Physics* **1972**, *56*, 2257-2261.
- 44. Miertuš, S.; Scrocco, E.; Tomasi, J., Electrostatic Interaction of a Solute with a Continuum. A Direct Utilizaion of Ab Initio Molecular Potentials for the Prevision of Solvent Effects. *Chemical Physics* **1981**, *55*, 117-129.
- 45. Miertuš, S.; Tomasi, J., Approximate Evaluations of the Electrostatic Free Energy and Internal Energy Changes in Solution Processes. *Chemical Physics* **1982**, *65*, 239-245.
- 46. Pascual-ahuir, J. L.; Silla, E.; Tuñon, I., Gepol: An Improved Description of Molecular Surfaces. Iii. A New Algorithm for the Computation of a Solvent-Excluding Surface. *Journal of Computational Chemistry* **1994**, *15*, 1127-1138.
- 47. Harada, I.; Takeuchi, H., Raman and Ultraviolet Resonance Raman Spectra of Proteins and Related Compounds. In *Spectroscopy of Biological Systems*, R. J. H. Clark, R. E. H., Ed. John Wiley & Son Ltd: Chichester, U.K., 1986; pp 113-175.
- 48. Scott, A. P.; Radom, L., Harmonic Vibrational Frequencies: An Evaluation of Hartree–Fock, Møller–Plesset, Quadratic Configuration Interaction, Density Functional Theory, and Semiempirical Scale Factors. *The Journal of Physical Chemistry* **1996**, *100*, 16502-16513.
- 49. Shafaat, H. S.; Kim, J. E., Resonance Raman Analysis of the Tryptophan Cation Radical. *The Journal of Physical Chemistry Letters* **2014**, *5*, 3009-3014.
- 50. Laury, M. L.; Carlson, M. J.; Wilson, A. K., Vibrational Frequency Scale Factors for Density Functional Theory and the Polarization Consistent Basis Sets. *Journal of Computational Chemistry* **2012**, 33, 2380-2387.
- 51. Yanai, T.; Tew, D. P.; Handy, N. C., A New Hybrid Exchange—Correlation Functional Using the Coulomb-Attenuating Method (Cam-B3lyp). *Chemical Physics Letters* **2004**, 393, 51-57.
- 52. Sodium Citrate Tribasic Dihydrate Product Information. sigmaaldrich.com (accessed August 2, 2021).

- 53. Phan, H. T.; Haes, A. J., Impacts of Ph and Intermolecular Interactions on Surface-Enhanced Raman Scattering Chemical Enhancements. *The Journal of Physical Chemistry C* **2018**, *122*, 14846-14856.
- 54. Xi, W.; Haes, A. J., Elucidation of Hepes Affinity to and Structure on Gold Nanostars. *Journal of the American Chemical Society* **2019**, *141*, 4034-4042.
- 55. Wei, H.; Huang, Q.; Vikesland, P. J., The Aromatic Amine Pka Determines the Affinity for Citrate-Coated Gold Nanoparticles: In Situ Observation Via Hot Spot-Normalized Surface-Enhanced Raman Spectroscopy. *Environmental Science & Technology Letters* **2019**, *6*, 199-204.
- 56. Nguyen, A. H.; Peters, E. A.; Schultz, Z. D., Bioanalytical Applications of Surface-Enhanced Raman Spectroscopy: De Novo Molecular Identification. *Reviews in Analytical Chemistry* **2017**, *36*, 20160037.
- 57. Siddhanta, S.; Narayana, C., Surface Enhanced Raman Spectroscopy of Proteins: Implications for Drug Designing. *Nanomaterials and Nanotechnology* **2012**, *2*, 1.
- 58. Kurouski, D.; Postiglione, T.; Deckert-Gaudig, T.; Deckert, V.; Lednev, I. K., Amide I Vibrational Mode Suppression in Surface (Sers) and Tip (Ters) Enhanced Raman Spectra of Protein Specimens. *The Analyst* **2013**, *138*, 1665.
- 59. Chi, Z.; Chen, X. G.; Holtz, J. S. W.; Asher, S. A., Uv Resonance Raman-Selective Amide Vibrational Enhancement: Quantitative Methodology for Determining Protein Secondary Structure†. *Biochemistry* **1998**, 37, 2854-2864.
- 60. Hernández, B.; Tinacci, L.; Coïc, Y.-M.; Chenal, A.; Cohen, R.; Sanchez-Cortes, S.; Ghomi, M., Tryptophan Tight Binding to Gold Nanoparticles Induces Drastic Changes in Indole Ring Raman Markers. *The Journal of Physical Chemistry C* **2018**, *122*, 13034-13046.
- 61. Sweeney, J. A.; Asher, S. A., Tryptophan Uv Resonance Raman Excitation Profiles. *The Journal of Physical Chemistry* **2002**, *94*, 4784-4791.
- 62. Haldorai, Y.; Yeon, S.-H.; Huh, Y. S.; Han, Y.-K., Electrochemical Determination of Tryptophan Using a Glassy Carbon Electrode Modified with Flower-Like Structured Nanocomposite Consisting of Reduced Graphene Oxide and Sno 2. *Sensors and Actuators B: Chemical* **2017**, 239, 1221-1230.
- 63. Rivera, J. J.; Liang, J. H.; Shimamura, G. R.; Shafaat, H. S.; Kim, J. E., Raman and Quantum Yield Studies of Trp48-D5 in Azurin: Closed-Shell and Neutral Radical Species. *The Journal of Physical Chemistry B* **2019**, *123*, 6430-6443.
- 64. Proniewicz, E.; Tąta, A.; Szkudlarek, A.; Świder, J.; Molenda, M.; Starowicz, M.; Ozaki, Y., Electrochemically Synthesized Γ-Fe2o3 Nanoparticles as Peptide Carriers and Sensitive and Reproducible Sers Biosensors. Comparison of Adsorption on Γ-Fe2o3 Versus Fe. *Applied Surface Science* **2019**, *495*, 143578.
- 65. Pajović, J. D.; Dojčilović, R.; Božanić, D. K.; Kaščáková, S.; Réfrégiers, M.; Dimitrijević-Branković, S.; Vodnik, V. V.; Milosavljević, A. R.; Piscopiello, E.; Luyt, A. S., et al., Tryptophan-Functionalized Gold Nanoparticles for Deep Uv Imaging of Microbial Cells. *Colloids and Surfaces B: Biointerfaces* **2015**, *135*, 742-750.
- 66. Szczerbiński, J.; Metternich, J. B.; Goubert, G.; Zenobi, R., How Peptides Dissociate in Plasmonic Hot Spots. *Small* **2020**, *16*, 1905197.
- 67. Kneipp, K., Chemical Contribution to Sers Enhancement: An Experimental Study on a Series of Polymethine Dyes on Silver Nanoaggregates. *The Journal of Physical Chemistry C* **2016**, *120*, 21076-21081.
- 68. Wang, R.; Shen, X.-R.; Zhang, M.; Devasenathipathy, R.; Pang, R.; Wu, D.-Y.; Zhang, J.; Ulstrup, J.; Tian, Z.-Q., Adsorption, Chemical Enhancement, and Low-Lying Excited States Ofp-Methylbenzenethiol on Silver and Gold Nanoparticle Surfaces: A Surface Enhanced Raman Spectroscopy and Density Functional Theory Study. *The Journal of Physical Chemistry C* **2019**, 123, 23026-23036.

- 69. Osawa, M.; Matsuda, N.; Yoshii, K.; Uchida, I., Charge Transfer Resonance Raman Process in Surface-Enhanced Raman Scattering from P-Aminothiophenol Adsorbed on Silver: Herzberg-Teller Contribution. *The Journal of Physical Chemistry* **2002**, *98*, 12702-12707.
- 70. Chenal, C.; Birke, R. L.; Lombardi, J. R., Determination of the Degree of Charge-Transfer Contributions to Surface-Enhanced Raman Spectroscopy. *ChemPhysChem* **2008**, 9, 1617-1623.
- 71. Lombardi, J. R.; Birke, R. L., A Unified Approach to Surface-Enhanced Raman Spectroscopy. *The Journal of Physical Chemistry C* **2008**, *112*, 5605-5617.
- 72. Valley, N.; Greeneltch, N.; Van Duyne, R. P.; Schatz, G. C., A Look at the Origin and Magnitude of the Chemical Contribution to the Enhancement Mechanism of Surface-Enhanced Raman Spectroscopy (Sers): Theory and Experiment. *The Journal of Physical Chemistry Letters* **2013**, *4*, 2599-2604.
- 73. Birke, R. L.; Lombardi, J. R.; Saidi, W. A.; Norman, P., Surface-Enhanced Raman Scattering Due to Charge-Transfer Resonances: A Time-Dependent Density Functional Theory Study of Ag13-4-Mercaptopyridine. *The Journal of Physical Chemistry C* **2016**, *120*, 20721-20735.
- 74. El-Khoury, P. Z.; Schultz, Z. D., From Sers to Ters and Beyond: Molecules as Probes of Nanoscopic Optical Fields. *The Journal of Physical Chemistry C* **2020**, *124*, 27267-27275.
- 75. Grys, D.-B.; de Nijs, B.; Salmon, A. R.; Huang, J.; Wang, W.; Chen, W.-H.; Scherman, O. A.; Baumberg, J. J., Citrate Coordination and Bridging of Gold Nanoparticles: The Role of Gold Adatoms in Aunp Aging. *ACS Nano* **2020**, *14*, 8689-8696.
- 76. Rani, M.; Moudgil, L.; Singh, B.; Kaushal, A.; Mittal, A.; Saini, G. S. S.; Tripathi, S. K.; Singh, G.; Kaura, A., Understanding the Mechanism of Replacement of Citrate from the Surface of Gold Nanoparticles by Amino Acids: A Theoretical and Experimental Investigation and Their Biological Application. *RSC Advances* **2016**, *6*, 17373-17383.
- 77. Perera, G. S.; Athukorale, S. A.; Perez, F.; Pittman, C. U.; Zhang, D., Facile Displacement of Citrate Residues from Gold Nanoparticle Surfaces. *Journal of Colloid and Interface Science* **2018**, *511*, 335-343.
- 78. Park, J.-W.; Shumaker-Parry, J. S., Structural Study of Citrate Layers on Gold Nanoparticles: Role of Intermolecular Interactions in Stabilizing Nanoparticles. *Journal of the American Chemical Society* **2014**, *136*, 1907-1921.

TOC graphic:

